

Individual Nanostructures in an Epsilon-Near-Zero Material Probed with 3D-Sculpted Light

Brian Kantor,^{1,2,3} Israel De Leon,^{3,4,5} Lisa Ackermann,^{6,7} and Peter Banzer^{1,2,3,7,8,*}

¹*Institute of Physics, University of Graz, Styria, Austria*

²*Christian Doppler Laboratory for Structured Matter Based Sensing,
Christian Doppler Forschungsgesellschaft, Styria, Austria*

³*Max Planck–University of Ottawa Centre for Extreme and Quantum Photonics,
Max Planck Gesellschaft–University of Ottawa, Ontario, Canada*

⁴*ASML Netherlands, North Brabant, Netherlands*

⁵*School of Engineering and Sciences, Tecnologico de Monterrey, Monterrey, Mexico*

⁶*Institute of Photonic Technologies, Friedrich-Alexander-Universität Erlangen-Nürnberg, Bavaria, Germany*

⁷*School of Advanced Optical Technologies, Friedrich-Alexander-Universität Erlangen-Nürnberg, Bavaria, Germany*

⁸*Max Planck Institute for the Science of Light, Max Planck Gesellschaft, Bavaria, Germany*

Epsilon-near-zero (ENZ) materials, i.e., materials with vanishing real part of the permittivity, have become an increasingly desirable platform for exploring linear and nonlinear optical phenomena in nanophotonic and on-chip environments. ENZ materials inherently enhance electric fields for properly chosen interaction scenarios, host extreme nonlinear optical effects, and lead to other intriguing phenomena. To date, studies in the optical domain mainly focused on nanoscopically thin films of ENZ materials and their interaction with light and other nanostructured materials. Here, the optical response of individual nanostructures milled into an ENZ material are explored both experimentally and numerically. For the study, 3D structured light beams are employed, allowing for the full utilization of polarization-dependent field enhancements enabled by a tailored illumination and a vanishing permittivity. This study reveals the underlying intricate interaction mechanisms and showcase the polarization-dependent controllability, paving the way towards experiments in the nonlinear optical regime where the presented effects will enable polarization-controlled nonlinear refractive index based ultra-fast switching on the single nanostructure level.

I. INTRODUCTION

Birthered from the metamaterials community, epsilon-near-zero (ENZ) materials have been pursued over the past two decades for their intriguing optical properties.^[1, 2] In the linear regime, ENZ materials have already shown to enable an array of optical processes ranging from enhanced spin-orbit coupling,^[3] to phase modulation in photonic waveguides,^[4] and tunneling through microwave cavities.^[5] Another unique facet of behavior specific to ENZ materials lies within transparent conducting oxides (TCOs) which possess a zero-crossing of their permittivity. TCOs, such as indium tin-oxide (ITO) in particular, allow for extreme refractive index changes by boosting the nonlinear response of the material due to the field enhancements promoted by the ENZ regime.^[6] Such nonlinear properties can be used for enhanced third-harmonic wave generation,^[7, 8] and is even being considered for purely passive phase modulators for silicon photonics technologies.^[9, 10] Even stronger nonlinear effects and refractive index changes have been realized by combining plasmonic nanostructures with unstructured isotropic ENZ films.^[11]

Despite the recent progress in characterizing the properties of the near-zero-permittivity regime,^[12, 13] the experimental study of ENZ materials in the form of either

individual or patterned nanostructures is largely unexplored so far. With the promising capabilities for significant nonlinear processes to take place on small footprints with ENZ materials,^[14, 15] it is important to understand and characterize the linear optical response of ENZ nanostructures. In this work, we thus study ENZ nanostructures, i.e., nanoholes milled into an ENZ film, in the linear optical regime illuminated with sculpted light beams. We choose the structure of the illumination such that it matches the cylindrical symmetry of the investigated nanostructures, while also allowing the realization of various interaction scenarios. We consider two orthogonal forms of structured beams^[16] whose cylindrical symmetry match that of the nanohole. It is shown that depending on the polarization of the incident beam, the transmission properties of the nanoholes contrast significantly. To the best of our knowledge, this is the first experimental study of the optical response of an individual nanostructure in an ENZ material. Furthermore, we also showcase, for the first time, the potential of vectorially structured light in the interaction of electromagnetic waves with an ENZ material. A hole geometry is considered due to its straightforward fabrication and symmetry overlap with the incident field profiles we utilize. As we will see later, symmetry plays a significant role in either maximizing or minimizing the unique polarization-dependent effects observed. By understanding the transmission properties of these holes in the linear regime, one can further explore nonlinear schemes in the future with sure footing.

* peter.banzer@uni-graz.at

II. INVESTIGATED SYSTEM

Prior to any structuring, an ITO film of 310 nm thickness sputtered on a 175 μm thick BK7 glass substrate^[17] was placed in an ellipsometer to obtain the complex refractive index. The zero-permittivity value of the real part exists when the refractive index n and the absorption coefficient k are equivalent, which in this case occurs at $\lambda = 1250$ nm. The film was then patterned with nanoholes via focused ion beam milling. An array of holes with varying diameters were milled in the ITO film. In order to maintain the permittivity measured by the ellipsometer, it is imperative to minimize fabrication side effects from the focused ion beam. This is mainly achieved by using the correct ion source, which was found to be neon as opposed to the conventional use of gallium.

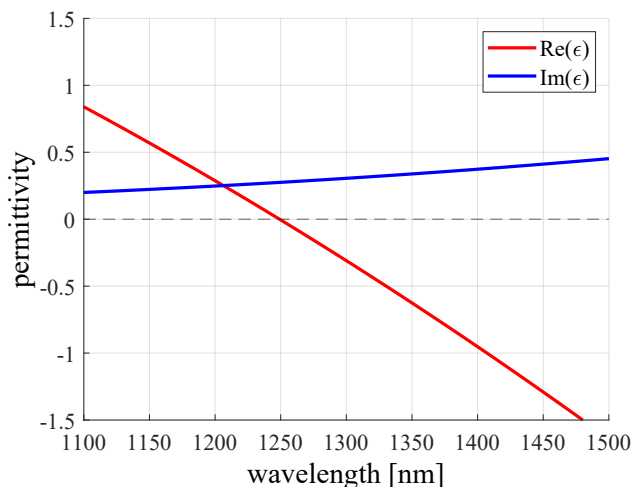


FIG. 1: Experimental ellipsometry data taken for the unstructured ITO film. The permittivity crosses zero at $\lambda = 1250$ nm. The nonzero imaginary component results in a complex refractive index of $n + ik = 0.38 + i0.38$ at this wavelength.

III. POLARIZATION- AND SYMMETRY-DRIVEN FIELD ENHANCEMENT

The key property used throughout this work is centered around the boundary conditions for the normal component of an electric field oscillating at an interface: $\epsilon_1 \mathbf{E}_{\perp,1} = \epsilon_2 \mathbf{E}_{\perp,2}$. Here the bulk properties of the two media are considered such that the surface charge density term σ can be neglected. Solving for the electric field in medium 2, where medium 1 is vacuum and medium 2 is the ENZ environment, the electric field takes the form: $\mathbf{E}_{\perp,2} = \frac{\epsilon_1}{\epsilon_2} \mathbf{E}_{\perp,1}$. As $\text{Re}(\epsilon_2) \rightarrow 0$, the normal component of the electric field in the ENZ environment diverges. Oftentimes, the polarization distribution of the incident field, in conjunction with the geometry of the ENZ structure,

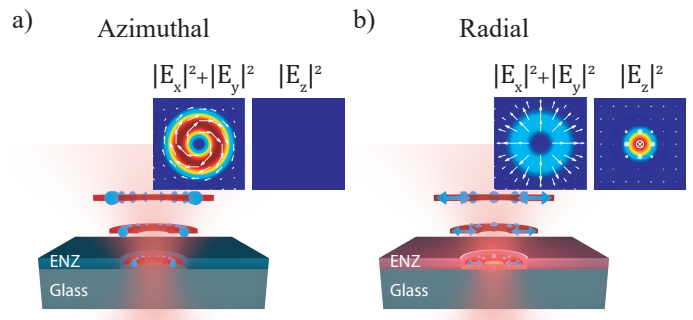


FIG. 2: A cross-sectional slice representing the two transverse field components focused onto an ENZ hole helps visualize the polarization-driven effects. The respective transverse and longitudinal electric field intensity distributions at the focus (in vacuum) are also shown as insets with electric field vectors as an overlay. a) The electric field distribution of the azimuthal field oscillates purely tangential to the ITO hole side-walls, resulting in no significant field enhancement. b) The transverse electric field contribution for the radially polarized field oscillates perpendicularly to the wall of the ENZ hole, yielding a field enhancement at all points along the interface.

is not configured for optimizing the field enhancement. Here we consider a geometry for the ENZ environment which overlaps symmetrically with the distribution of the electric field while examining sets of polarization states which either maximize or minimize the field enhancement. The structure which naturally facilitates a symmetric overlap is a cylindrical void in the ENZ medium. In order to obey the symmetry of the nanohole while probing the polarization-tailored responses, we individually excite each nanohole with either an azimuthally or radially polarized cylindrical vector beam.^[16, 18] For a brief phenomenological interpretation, we only consider an interaction when the electric field distribution is perfectly centered with the nanohole, i.e., the optical axis of the beam being aligned with the symmetry axis of the hole. Under tight focusing, the azimuthally polarized beam retains qualitatively the focal electric field distribution in the transverse plane, where the electric field components oscillate tangential to the interior hole interface (Figure 2a). The tightly focused radially polarized beam in contrast leads to a more complex focal electric field distribution. It results in a 3-dimensional focal electric field with the transverse components maintaining a radial polarization distribution, overlaid with a strong field component oscillating in the longitudinal direction.^[19–21] Depending on the hole diameter, the longitudinal field can either interact strongly with the surface of the ENZ film, or overlap and interact with the glass substrate leaving any interaction with the ENZ to the transverse field. In any case, for the radially polarized field, any field component which interacts with the ENZ interface will do so

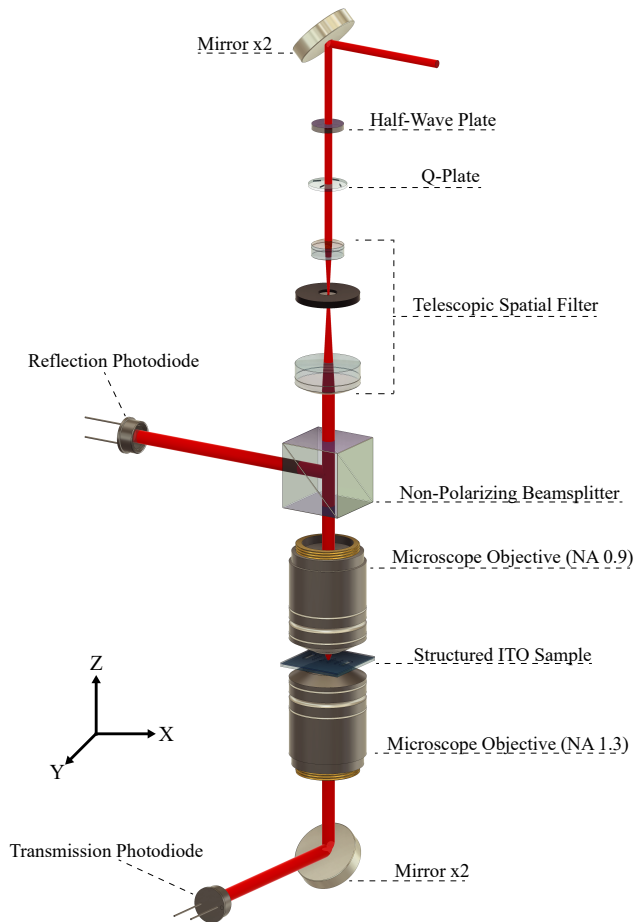


FIG. 3: Experimental setup detailing the polarization structuring and tight focusing onto the structured ITO sample. The ITO sample is mounted to a 3D piezo stage (not depicted here) allowing for precise alignment of the nanoholes with respect to the focal field.

in a manner perpendicular to the interface itself, resulting in a field enhancement as indicated in Figure 2b.

IV. EXPERIMENT

The experimental setup begins with a super-continuum light source whose wavelength is selected using a liquid crystal wavelength filter. The output of the filter produces a beam with a wavelength of 1250 nm and a bandwidth of ~ 7 nm. The beam passes through a single mode fiber to both guide the beam towards the main setup while also filtering the spatial mode of the incident field. Out of the fiber, the beam is launched into a tower configuration and guided to the top.^[22] The field is first structured using a linear polarizer and a liquid-crystal-based q-plate, which allows one to either structure the beam to carry a radial or azimuthal polarization distribution.^[23] A spatial filter is then placed shortly after to remove un-

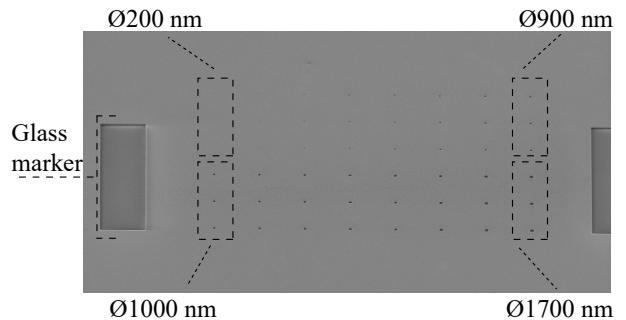


FIG. 4: Scanning-electron micrograph of the milled nanoholes in the ITO film. For each hole diameter, two duplicate holes are milled. The hole diameters range from 200 nm to 1700 nm and are spaced 20 μm apart to allow for the experimental study of individual nanoholes without the illuminating beam overlapping with neighbouring structures.

desired higher-order spatial modes, refining the quality of the structured beam. The filtered structured beam transmits through a non-polarizing beam splitter (NPBS) and is focused by a microscope objective with numerical aperture (NA) of 0.9. The field is tightly focused to a spot size on the order of the wavelength and interacts with the structured ITO sample which sits on a 3D piezo table. Light transmitted through the sample is collected with a 1.3 NA oil immersion objective, which due its confocal alignment, guides the collimated output towards a photodiode. Reflected light passes back through the focusing objective and reflects off the NPBS towards the reflection photodiode. While the end measurement data comes from the transmitted field, the measured reflected field is used for ensuring precise alignment between the focal field and the nanostructures.

The nanoholes were fabricated using focused ion beam milling (Figure 4). Neon ions were used to mill the holes, with diameters ranging from 200 nm to 1700 nm. This diameter range envelops the spot size for both the radial and azimuthal beams, allowing us to observe the transmission for nanoholes both smaller and larger than the focal field. Three identical holes are milled per column in case a fabrication fault occurs for a given hole. The holes are spaced 20 μm apart from each other to ensure no near-field excitation can take place. The measurement is done by performing a raster scan of the nanohole across the focal field with the use of the piezo stage. The resulting measurement is a scan image where each pixel corresponds to the relative power either reflected or transmitted for the beam with respect to the sample. The transmission images are normalized with respect to the glass substrate underneath the ITO film.

The scan images allow us to realize various interaction scenarios and to relate the interaction strength with the field profile at the focus. The center of the scan image represents the transmitted power for the beam centered with the hole (referred to as on-axis position or illumi-

nation). When considering nanoholes in conductors such as silver, a waveguide interpretation can be assigned to model the transmission properties of these holes.^[24] Due to the enhancement effects of the field in the ENZ regime, such a model fails to hold fully in our case and therefore numerical modelling is performed with the help of finite-difference-time-domain (FDTD) simulations. We mimic the experimental measurement procedure in our FDTD environment by raster scanning the nanohole on a glass substrate across a given structured focal field and collect the transmitted power with a field monitor.

V. RESULTS

With the individual holes scanned in transmission, a qualitative and quantitative comparison between polarization distributions can be made for the transmission properties of these holes. For the radially polarized field, a striking feature in the transmission arises for hole diameters between 800 – 1200 nm. For on-axis illumination, the transmission stays almost constant in this region of hole diameters, indicated by both the scan images and the transmission plot (Figures 5 & 6a). The hole diameters where this effect occurs corresponds with the walls of the ITO hole overlapping spatially with the transverse field components of the focal field. This suggests that the suppressed transmission occurs when the transverse fields can strongly interact with the ITO. For the radially polarized field distribution, this indicates that the transverse field is oscillating normal to the ITO wall in all directions, generating a field enhancement in the ITO surrounding the hole. As the holes become large enough such that the transverse field components no-longer interact strongly with the ITO, the transmission begins to restore. It is worth noting here that even for the largest hole diameter studied in the experiment and numerically (1700 nm), the tightly focused beam still overlaps with the ITO film for the chosen propagation parameters (NA, wavelength, etc.) for on-axis illumination. Thus, the recorded transmission still grows and does not reach yet a constant value for the largest holes tested (see Figure 6a).

The results achieved for an azimuthally polarized input beam, however, contrast significantly with those for the radially polarized field (Figure 5). For most of the hole diameters, the on-axis transmission remains the most prominent in the performed scans. Only for smaller diameters, the on-axis transmission is lower than for off-axis illumination (e.g., at 800 nm). The on-axis transmission plotted with dependence on the hole diameter also indicates a similar behavior in the experimental and simulated data (Figure 6b). For the azimuthally polarized field, the electric field in the interaction region is always parallel to the air-ITO interfaces for perfect on-axis illumination, both with respect to the upper ITO surface and the ITO side walls. Hence, no normal field component is present, which might get enhanced by the

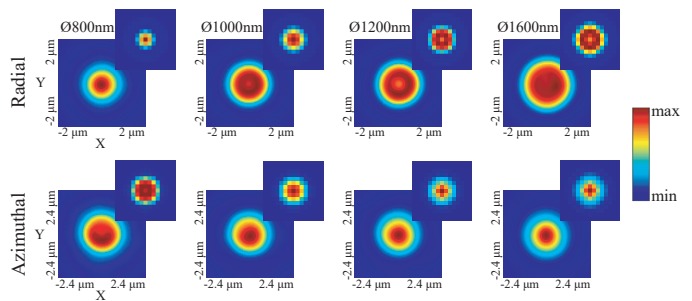


FIG. 5: Experimental and simulated (insets) scan images spanning a selection of holes over the region of interest for an incident radially and azimuthally polarized beam. The central pixels represent purely on-axis transmission, which in both experiment and simulation show a dip for the radially polarized beam for a select range of hole diameters. The transmission values are normalized to the transmission through the bare glass substrate with no ITO present.

ENZ material.

To better gauge how the focal fields interact with the ENZ nanostructure, we performed a detailed numerical inspection of the electric fields and the energy flux (Poynting vector) in the interaction region. We show the corresponding cross-sections for a 1200 nm diameter hole illuminated by both a tightly focused radially and azimuthally polarized field (see Figure 7). This hole diameter is considered due to the observed contrast in transmission between the two beams occurring here, and because for both beams the focal spot size is roughly equivalent to this diameter. Due to the strong lateral confinement of the longitudinal field for the radially polarized focal field, it primarily interacts with the glass substrate, leaving any interaction with the ITO purely to the transverse field components oscillating perpendicular (normal) to the walls of the ITO. The electric field amplitude is enhanced at the wall and decays as the field extends into the ITO. The Poynting vector illustrated as white arrows in Figure 7 features an enhanced transverse component in the corresponding region close to the side walls. Hence, the energy flowing through the hole and being detected in forward direction should be reduced significantly. This observation is consistent with the measured suppressed transmission for on-axis illumination (compare plateau region in Figure 6a).

The electric field profile for the azimuthal beam is shown to be guided primarily through the hole, hardly influenced by the ITO material. The maximum electric field amplitude remains to the free-space spatial mode, and no field enhancements are observed in the ITO. The Poynting vectors again support the observed behavior which was measured for this system. The energy dominantly flows along the optical axis with transverse vector components being a consequence of the convergence/divergence properties of the focusing objective. An

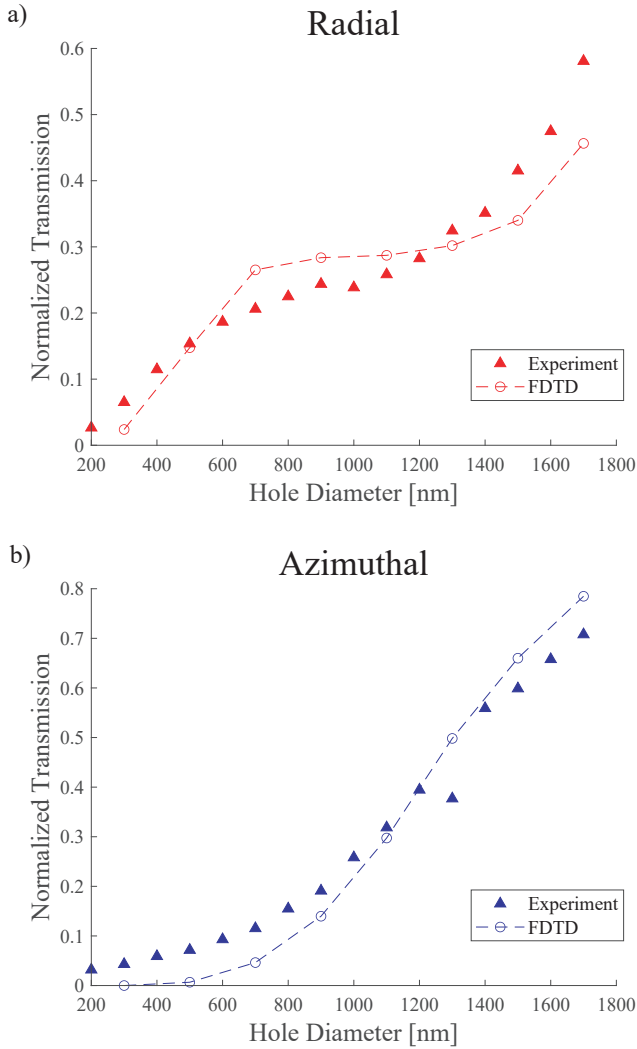


FIG. 6: a) Transmission plot for the radially polarized beam focused on-axis with the center of the nanoholes. A plateau occurs for hole diameters near the spot size of the focal field. This region also facilitates the strongest field enhancements observed in FDTD. b) Same measurement but for an azimuthally polarized focal field. The transmission experiences no such plateau and no field enhancements are expected in the ITO.

increased transverse energy flow resulting from the light-ITO interaction is not observed.

The field dynamics shown in the FDTD results indicate agreement with the experimentally observed transmission properties of the nanoholes. When considering hole diameters much smaller than the spot size of the focal field (< 800 nm), the interaction with the radially polarized field is significantly affected (Figure 8). In this scenario, the longitudinal component, which interacts with the upper surface of the ITO layer, contributes to the field enhancement as well. These enhanced field components modify the total Poynting vector distribution

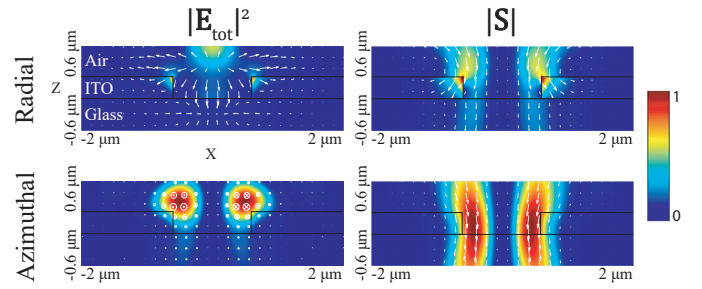


FIG. 7: Cross-sectional view of the simulated time-averaged electric field intensity and Poynting field across a 1200 nm hole for both a tightly focused radially and azimuthally polarized beam. Electric field vectors and Poynting vectors are shown for a snapshot in time (overlays). The Poynting vectors diverge from the optical axis for the incident radial beam, whereas the azimuthal beam maintains the energy flow in the direction of propagation. The amplitudes in each sub-figure are normalized to their respective maxima.

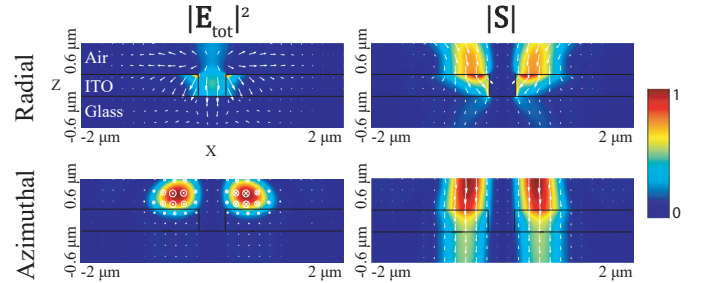


FIG. 8: Cross-sectional view of the simulated time-averaged electric field intensity and Poynting field across a 400 nm hole for both a tightly focused radially and azimuthally polarized beam. Electric field vectors and Poynting vectors are shown for a snapshot in time (overlays). The Poynting vectors show convergence towards the optical axis for the radial beam, whereas the azimuthal beam maintains the energy flow in the direction of propagation. The amplitudes in each sub-figure are normalized to their respective maxima.

in the ITO layer, resulting in a net energy flow which converges towards the optical axis, as opposed to larger holes whose Poynting vectors point away from the optical axis. It is only once the hole diameter is large enough to neglect the interaction between strong longitudinal field and ITO, while still being small enough to facilitate the interactions with the transverse field components, that the energy is partially redirected transversely into the ITO film and the transmission drops.

VI. CONCLUSION

The unique consequences of the boundary conditions for an ENZ medium indeed give rise to significant contrasting effects depending on the structure of the medium and the polarization distribution of the incoming excitation field. For nanoholes in an ENZ film, focal fields with cylindrical symmetry can either lead to strong boundary-driven field enhancement effects or completely suppress them depending on the polarization. This behavior was experimentally shown and numerically verified here for tightly focused radially and azimuthally polarized field distributions incident on such holes. Already in the linear optics regime, the contrasting transmission properties enabled by the ENZ structure and focal field provide a suitable environment for polarization-based optical switching schemes. Other structures, such as co-axial nanoholes, may also serve useful by allowing the longitudinal component of a focused radially polarized beam to fully interact with the ITO surface. Furthermore, the results serve as a basis for exploring next steps in the nonlinear regime, where significant nonlinear refractive index changes occur which are facilitated by the field enhancement mechanisms discussed above. Under the construction used here, these field-enhancement-driven refractive index changes could be achieved with substantially less incident power due to taking advantage of the

polarization-dependent field enhancement by the ENZ structure, resulting in efficient polarization-enabled all-optical switches and routers.

ACKNOWLEDGEMENTS

The financial support by the Austrian Federal Ministry of Labour and Economy, the National Foundation for Research, Technology and Development and the Christian Doppler Research Association is gratefully acknowledged. We thank Victor Deinhart and Katja Höflich for the fabrication of the investigated samples.

CONFLICT OF INTEREST

The authors declare no conflicts of interest.

DATA AVAILABILITY STATEMENT

Data regarding the results presented in this article are not publicly available at this time but may be obtained from the authors upon reasonable request.

-
- [1] A. Alu, M. G. Silveirinha, A. Salandrino, and N. Engheta, Epsilon-near-zero metamaterials and electromagnetic sources: Tailoring the radiation phase pattern, *Physical Review B* **75**, 155410 (2007).
- [2] R. Maas, J. Parsons, N. Engheta, and A. Polman, Experimental realization of an epsilon-near-zero metamaterial at visible wavelengths, *Nature Photonics* **7**, 907 (2013).
- [3] J. S. Eismann, L. Ackermann, B. Kantor, S. Nechayev, M. Z. Alam, R. Fickler, R. W. Boyd, and P. Banzer, Enhanced spin-orbit coupling in an epsilon-near-zero material, *Optica* **9**, 1094 (2022).
- [4] I. C. Reines, M. G. Wood, T. S. Luk, D. K. Serkland, and S. Campione, Compact epsilon-near-zero silicon photonic phase modulators, *Optics Express* **26**, 21594 (2018).
- [5] M. Silveirinha and N. Engheta, Tunneling of electromagnetic energy through subwavelength channels and bends using ϵ -near-zero materials, *Physical Review Letters* **97**, 157403 (2006).
- [6] M. Z. Alam, I. De Leon, and R. W. Boyd, Large optical nonlinearity of indium tin oxide in its epsilon-near-zero region, *Science* **352**, 795 (2016).
- [7] T. S. Luk, D. De Ceglia, S. Liu, G. A. Keeler, R. P. Prasankumar, M. A. Vincenti, M. Scalora, M. B. Sinclair, and S. Campione, Enhanced third harmonic generation from the epsilon-near-zero modes of ultrathin films, *Applied Physics Letters* **106** (2015).
- [8] D. de Ceglia, M. A. Vincenti, N. Akozbek, M. J. Bloemer, and M. Scalora, Nested plasmonic resonances: extraordinary enhancement of linear and nonlinear interactions, *Optics Express* **25**, 3980 (2017).
- [9] Y. Sha, Z. T. Xie, J. Wu, H. Fu, and Q. Li, All-optical switching in epsilon-near-zero asymmetric directional coupler, *Scientific Reports* **12**, 17958 (2022).
- [10] J. Navarro-Arenas, J. Parra, and P. Sanchis, Ultrafast all-optical phase switching enabled by epsilon-near-zero materials in silicon, *Optics Express* **30**, 14518 (2022).
- [11] M. Z. Alam, S. A. Schulz, J. Upham, I. De Leon, and R. W. Boyd, Large optical nonlinearity of nanoantennas coupled to an epsilon-near-zero material, *Nature Photonics* **12**, 79 (2018).
- [12] X. Niu, X. Hu, S. Chu, and Q. Gong, Epsilon-near-zero photonics: a new platform for integrated devices, *Advanced Optical Materials* **6**, 1701292 (2018).
- [13] S. Campione, I. Brener, and F. Marquier, Theory of epsilon-near-zero modes in ultrathin films, *Physical Review B* **91**, 121408 (2015).
- [14] O. Reshef, I. De Leon, M. Z. Alam, and R. W. Boyd, Nonlinear optical effects in epsilon-near-zero media, *Nature Reviews Materials* **4**, 535 (2019).
- [15] M. A. A. Abouelatta, A. Safari, M. Z. Alam, X. Garcia-Santiago, D. Beutel, L. Cheng, R. W. Boyd, C. Rockstuhl, and R. Alaei, Optically tunable bianisotropy in a sphere made from an epsilon-near-zero material, *Optics Letters* **48**, 783 (2023).
- [16] H. Rubinsztein-Dunlop, A. Forbes, M. V. Berry, M. R. Dennis, D. L. Andrews, M. Mansuripur, C. Denz, C. Alpmann, P. Banzer, T. Bauer, E. Karimi, L. Marrucci, M. Padgett, M. Ritsch-Martel, N. M. Litchinitser, N. P. Bigelow, C. Rosales-Guzmán, A. Belmonte, J. P. Torres, T. W. Neely, M. Baker, R. Gordon, A. B. Stil-

- goe, J. Romero, A. G. White, R. Fickler, A. E. Willner, G. Xie, B. McMorrán, and A. M. Weiner, Roadmap on structured light, *Journal of Optics* **19**, 013001 (2016).
- [17] Präzisions glas & optik gmbh, <https://www.pgo-online.com>.
- [18] Q. Zhan, Cylindrical vector beams: from mathematical concepts to applications, *Advances in Optics and Photonics* **1**, 1 (2009).
- [19] R. Dorn, S. Quabis, and G. Leuchs, Sharper focus for a radially polarized light beam, *Physical Review Letters* **91**, 233901 (2003).
- [20] M. Eberler and O. Glöckl, Focusing light to a tighter spot, *Optics Communications* **179**, 1 (2000).
- [21] K. S. Youngworth and T. G. Brown, Focusing of high numerical aperture cylindrical-vector beams, *Optics Express* **7**, 77 (2000).
- [22] P. Banzer, U. Peschel, S. Quabis, and G. Leuchs, On the experimental investigation of the electric and magnetic response of a single nano-structure, *Optics Express* **18**, 10905 (2010).
- [23] L. Marrucci, C. Manzo, and D. Paparo, Optical spin-to-orbital angular momentum conversion in inhomogeneous anisotropic media, *Physical Review Letters* **96**, 163905 (2006).
- [24] J. Kindler, P. Banzer, S. Quabis, U. Peschel, and G. Leuchs, Waveguide properties of single subwavelength holes demonstrated with radially and azimuthally polarized light, *Applied Physics B* **89**, 517 (2007).